Cell Reports, Volume *43*

Supplemental information

HIF1α-dependent uncoupling of glycolysis suppresses tumor cell proliferation

Andrés A. Urrutia, Claudia Mesa-Ciller, Andrea Guajardo-Grence, H. Furkan Alkan, Inés Soro-Arnáiz, Anke Vandekeere, Ana Margarida Ferreira Campos, Sebastian Igelmann, Lucía Fernández-Arroyo, Gianmarco Rinaldi, Doriane Lorendeau, Katrien De Bock, Sarah-Maria Fendt, and Julián Aragonés

Figure S1

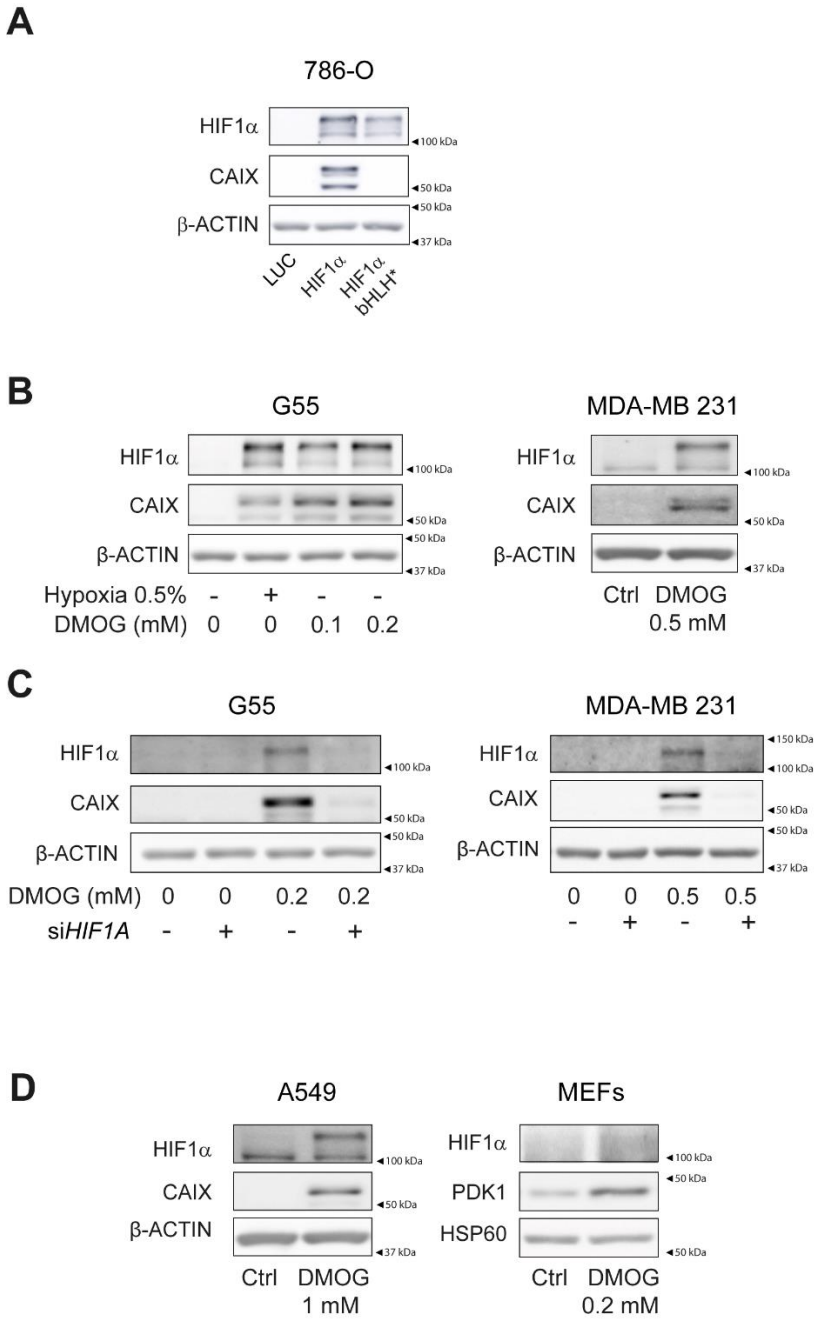

Figure S1. Protein analysis of HIF1α and HIF1-dependent target genes in hypoxia-exposed and DMOG-treated cells, related to Figure 1 and 2.

(A) Representative western blot analysis of the HIF1α, CAIX and β-ACTIN protein in 786-O-HIF1α and HIF1α-bHLH* cells, and in their corresponding control cells. (B) Representative western blot analysis of the HIF1α, CAIX and β-ACTIN protein in G55 control cells and in G55 cells exposed to hypoxia 0.5% and treated with DMOG 0.1 or 0.2 mM (left panel). Representative western blot analysis of the HIF1α, CAIX and β-ACTIN protein in MDA-MB-231 control cells and MDA-MB-231 treated with DMOG 0.5 mM (right panel). (C) Representative western blots of the HIF1α, CAIX and β-ACTIN protein in G55 or MDA-MB-231 control cells, HIF1α-silenced G55 or MDA-MB-231 cells, G55 or MDA-MB-231 cells treated with DMOG, and HIF1α-silenced G55 or MDA-MB-231 cells treated with DMOG. (D) Representative western blots of the HIF1α, CAIX and β-ACTIN protein in A549 control cells and A549 treated with DMOG 1 mM, and of the HIF1α, PDK1 and HSP60 protein in MEFs exposed to DMOG 0.2 mM or untreated.

Figure S2

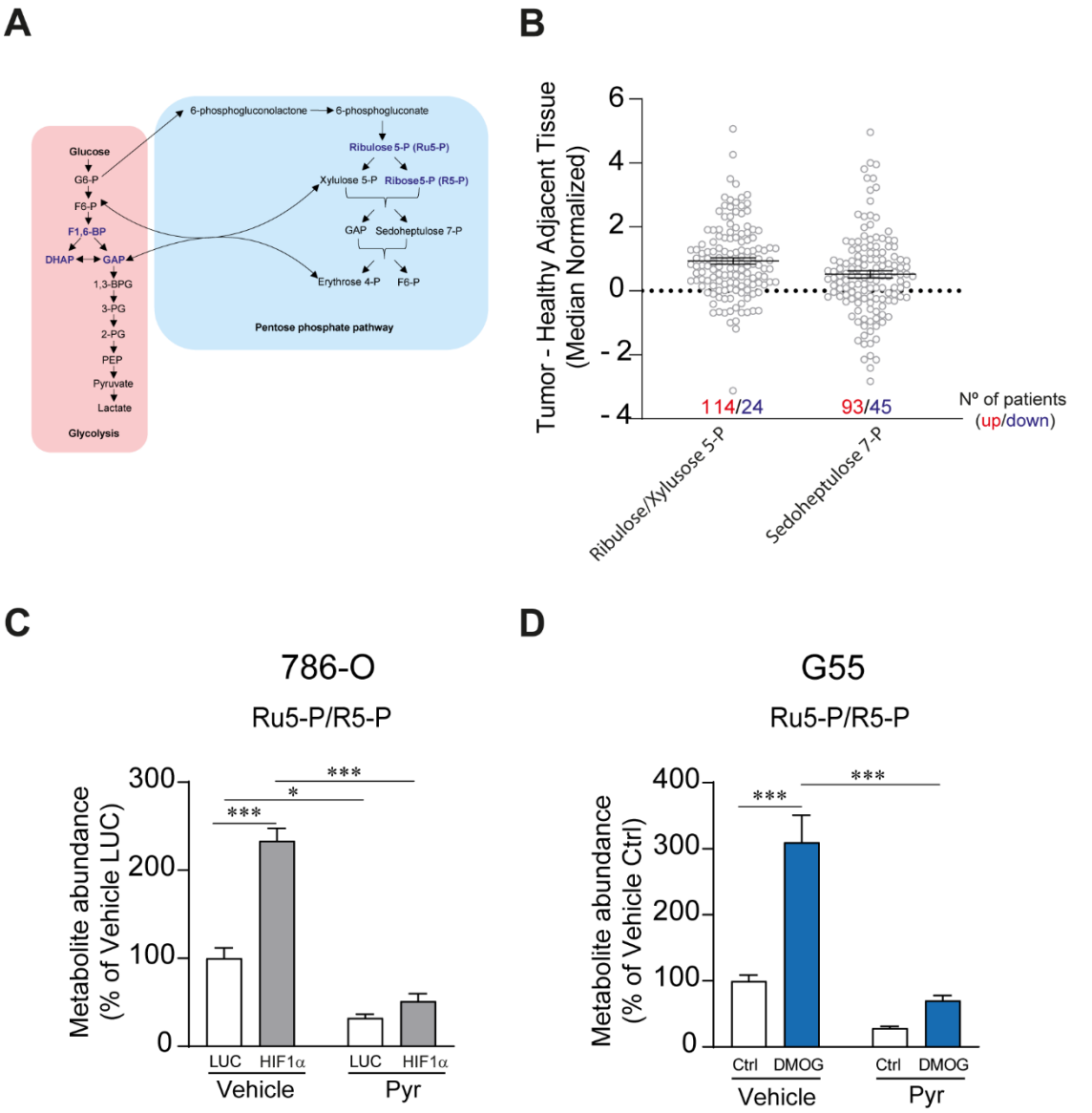

Figure S2. Accumulation of upper glycolytic and pentose phosphate metabolites as a consequence of HIF1α-dependent lower glycolysis inhibition, related to Figure 3.

(A) The scheme shows the metabolic pathways connecting upper glycolysis and the pentose phosphate pathway. Metabolites measured in Figures 3H-3K, S2C, and S2D are indicated in blue. (B) Relative induction of pentose phosphate metabolites in 138 human VHL-deficient renal cell carcinomas relative to their adjacent kidney tissue. The graph shows those samples in which metabolite fold induction is positive (red) and negative (blue). (C) Relative amount of pentose 5-phosphate metabolites (pool of ribose 5-phosphate + ribulose 5-phosphate) in 786-O-HIF1α cells and their corresponding control cells in the presence or absence of extracellular pyruvate 1 mM (n=3). (D) Relative amount of pentose 5-phosphate metabolites (pool of ribose-5-phosphate, R5-P + ribulose-5-phosphate, Ru5-P) in G55 control cells and G55 cells treated with DMOG 0.2 mM, in the presence or absence of extracellular pyruvate 1 mM (n=3). In the bar graphs, the values represent the mean ± SEM and the statistical analysis was performed using a two-way ANOVA followed by Tukey's post hoc test: *p < 0.05 and ***p< 0.001 represent significant p-values.

Figure S3

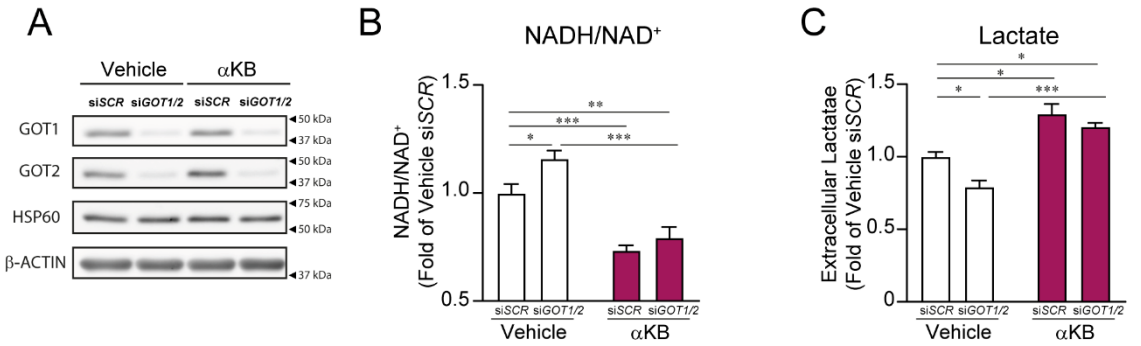

Figure S3. NADH/NAD⁺-dependent inhibition of lactate release in GOT1/2-silenced cells, related to Figure 5.

(A) Representative western blot of GOT1, GOT2, HSP60 and β-ACTIN proteins in GOT1/2-silenced G55 cells and their corresponding control cells (siSCR), in the presence or absence of extracellular αKB (1 mM). (B) NADH/NAD⁺ ratio in GOT1/2-silenced G55 cells and their corresponding control cells in the presence or absence of extracellular αKB (1 mM) (n=5-6). (C) The relative amount of extracellular lactate released by GOT1/2-silenced G55 cells and their corresponding control cells in the presence or absence of extracellular αKB (1 mM) (n=5-6). In the bar graphs, the values represent the mean ± SEM and the statistical analysis was performed using two-way ANOVA followed by Tukey's post hoc test: *$p < 0.05$, **$p < 0.01$, ***$p < 0.001$.